ISSN 0006-2979, Biochemistry (Moscow), 2025, Vol. 90, No. 11, pp. 1741-1756 © Pleiades Publishing, Ltd., 2025.
Russian Text © The Author(s), 2025, published in Biokhimiya, 2025, Vol. 90, No. 11, pp. 1862-1878.

# Activity of METTL4 Methyltransferase Is Crucial for Maintaining Optimal Splicing Efficiency in HeLa S3 Cells

**Anastasiia K. Bolikhova[1,2,3,a*#], Andrey I. Buyan[3,4#], Maria A. Khokhlova[1,3], Sofia S. Mariasina[2,3,5], Anton R. Izzi[1,6], Alexander Y. Rudenko[2], Marina V. Serebryakova[2], Alexander M. Mazur[7], Olga A. Dontsova[1,2,3,8], and Petr V. Sergiev[1,2,3]**

[1]*Skolkovo Institute of Science and Technology, Center for Life Sciences, 121205 Skolkovo, Russia*

[2]*Belozersky Institute of Physico-Chemical Biology, Lomonosov Moscow State University, 119991 Moscow, Russia*

[3]*Department of Chemistry, Lomonosov Moscow State University, 119991 Moscow, Russia*

[4]*Institute of Protein Research, Russian Academy of Sciences, 142290 Pushchino, Moscow Region, Russia*

[5]*Research and Educational Resource Center "Pharmacy", RUDN University, 117198 Moscow, Russia*

[6]*Faculty of Bioengineering and Bioinformatics, Lomonosov Moscow State University, 119991 Moscow, Russia*

[7]*Institute of Bioengineering, Research Center of Biotechnology of the Russian Academy of Sciences, 119071 Moscow, Russia*

[8]*Department of Functioning of Living Systems, Shemyakin-Ovchinnikov Institute of Bioorganic Chemistry, Russian Academy of Sciences, 117997 Moscow, Russia*

[a]*e-mail: anastasia_b7@mail.ru*

Received August 8, 2025
Revised November 11, 2025
Accepted November 13, 2025

**Abstract**—Methyltransferases that modify spliceosomal small nuclear RNAs (snRNAs) play a crucial role in the cell by ensuring proper maturation of snRNAs, which is essential for optimal function of spliceosome. In this study, we investigated the enzyme METTL4, which catalyzes N6-methylation of 2′-O-methyladenosine at position 30 of U2 snRNA. Function of both the protein and the modification in splicing remains unclear. We demonstrated that inactivation of the *METTL4* gene in HeLa S3 cells leads to significant changes in alternative splicing, general slowdown in spliceosome activity, and intron accumulation. In the cells lacking METTL4, expression of the set of genes associated with ribosomal RNA maturation is reduced, and the number of coilin-positive structures, most likely Cajal bodies, is decreased in the nuclei of these cells.

**DOI**: 10.1134/S0006297925602382

*Keywords*: splicing, small nuclear RNAs (snRNAs), METTL4, U2 snRNA, methylation

## INTRODUCTION

N6-methyladenosine ($m^6A$) is one of the most common modified nucleotides in eukaryotic RNA [1]. $m^6A$ is found in various types of RNA, including messenger RNA (mRNA), transfer RNA (tRNA), ribosomal RNA (rRNA), long non-coding RNAs, and small nuclear RNAs (snRNAs) [2-6].

Addition of a methyl group to the N6 atom of adenosine could perform diverse regulatory functions depending on position of the nucleotide and type of the modified RNA. In the nucleus, the pattern of $m^6A$ distribution in pre-mRNA correlates with different

* To whom correspondence should be addressed.
# These authors contributed equally to this study.

splicing rates of introns [7]; in the cytoplasm, recognition of $m^6A$ could either enhance translation efficiency or lead to mRNA degradation [8, 9].

In the case of non-coding RNAs, modifications, including $m^6A$, could play regulatory and functional roles. For example, cessation of N6-methylation of A1832 in 18S rRNA or A4220 in 28S rRNA disrupts ribosome assembly, which, in turn, affects translation efficiency [10, 11]. The modified $m^6A43$ residue in U6 snRNA directly participates in splicing by stabilizing interaction between the U6 snRNA and the 5′ splice site [12, 13].

The range of enzymes that perform N6-methylation of adenosine is extremely diverse [14]. The methyltransferase complex METTL3–METTL14, which has several RNA targets and is involved in regulation of cell differentiation, is well studied [15]. Another such methyltransferase is METTL4, whose function has not yet been fully deciphered. The role of this enzyme, according to the current understanding, may vary depending on the type and state of the cell. Under hypoxia, METTL4 causes DNA methylation, regulating the cluster of genes associated with hypoxia response [16, 17]. Formation of $m^6A$ in the mitochondrial DNA by METTL4 plays an important role in the development of inflammation [18]. METTL4 can methylate mRNA and microRNA under certain conditions [19, 20]. However, the constitutive and evolutionarily conserved function of METTL4 is formation of $m^6Am$ from 2′-O-methyladenosine (Am) at position 30 of U2 snRNA [21, 22]. In some organisms, such as worms and fruit flies, the enzyme that 2′-O-methylates the 30th adenine in U2 snRNA is absent, and METTL4 orthologs modify A30 instead of Am30 [23, 24]. The 30th adenine of U2 snRNA is located immediately upstream the branch point recognition site [25], making modification of this residue a potential mechanism for regulating efficiency and accuracy of splicing. At the later stages of splicing, $m^6Am30$ is located next to the duplex formed by the complementary parts of U2 and U6 [26], potentially affecting stability and conformation of the U2–U6 complex.

In this work, we aimed to study how inactivation of the gene encoding the METTL4 protein affects HeLa S3 cells. We confirmed earlier observations that disappearance of METTL4 in human cells leads to cessation of N6-methylation of Am30 in U2 snRNA [27]. We demonstrated significant changes in alternative splicing in the HeLa S3 Δ*METTL4* cell line, showed that inactivation of *METTL4* is accompanied by the decrease in the number of Cajal bodies (CBs), and general decrease in the accuracy and efficiency of splicing. Thus, METTL4 appears to play an important role in maturation of the U2 snRNA, and its activity is important for optimal functioning of the spliceosome.

## MATERIALS AND METHODS

**Oligonucleotide synthesis.** All oligonucleotides (primers, probes) were synthesized by Lumiprobe LLC (Russia and EU); all sequences are provided in Table S1 in the Online Resource 1.

**Cell culturing.** HeLa S3 cells were cultured in a DMEM/F12 medium (Gibco, USA). Before use, the medium was supplemented with fetal bovine serum (50 mL per 500 mL of medium; Gibco), a mixture of penicillin and streptomycin antibiotics (5 mL per 500 mL of medium; Gibco), and GlutaMAX (5 mL per 500 mL of medium; Gibco). Cells were cultured at 37°C, 5% $CO_2$. Passaging was performed by scraping upon reaching 70-80% confluency.

**Inactivation of *METTL4* gene.** The *METTL4* gene was inactivated in the HeLa S3 cell line using the CRISPR-Cas9 method. A guide RNA (gRNA) sequence was generated using CRISPR guide RNA design (https://benchling.com). This gRNA (5′-GGAGCCGTTCGTAATGCGAG-3′) targets exon 4. Sense and antisense oligonucleotides (MET4_hum_CrF and MET4_hum_CrR) were annealed and cloned into a pX458 vector (Addgene: 48138) [28].

HeLa S3 cells were transfected with the plasmid using a Lipofectamine™ 3000 reagent (Invitrogen, USA). After 48 h, GFP-positive cells were sorted using a BD FACSAria™ III (BD Biosciences, USA) and plated as single clones. Individual clones were analyzed by PCR (MET4_hum_ChF and MET4_hum_ChR) and Sanger sequencing of the target region.

**Western blotting.** The following antibodies were used to detect proteins: anti-METTL4 (Invitrogen), anti-GAPDH (Abcam, UK).

**Isolation and analysis of U2 snRNA.** Total RNA was isolated from cells using an ExtractRNA reagent (Evrogen, Russia). U2 snRNA was isolated using a 5′-biotinylated oligonucleotide (U2_BIO), as described in Laptev et al. [29] and in the Supplementary Methods section in the Online Resource 1.

**Fluorescence *in situ* hybridization (FISH).** DNA probes complementary to U2 snRNA targets and labeled with Cy5 fluorescent dye were designed. HeLa S3 cells were seeded onto poly-lysine slides, fixed with a fresh 4% paraformaldehyde (PFA) solution. Cells were permeabilized in PBS (Sigma-Aldrich, USA) containing 0.01% Triton X-100. Background blocking was performed with a 1% glycine solution in PBS. Pre-hybridization was carried out in a ULTRAhyb™-Oligo buffer (Thermo Fisher Scientific, USA); hybridization was performed in the same buffer with addition of 100 ng of probe. After washing, cells were stained with a mixture of DAPI (1 mg/mL) and Mowiol (1 : 1000; Sigma-Aldrich). Samples were analyzed using a Celena X fluorescence microscope (Logos Biosystems, South Korea). The staining protocol is detailed

in the Supplementary Methods section in the Online Resource 1.

**Immunofluorescence of Cajal Bodies.** HeLa S3 cells were seeded onto poly-lysine slides. Cells were fixed with a 4% PFA solution. Cells were permeabilized in PBST (PBS containing 0.05% Tween-20) and blocked with a 1% bovine serum albumin solution in PBST. Cells were stained with primary antibodies against coilin (Abcam) and secondary antibodies against rabbit antibodies labeled with Cy5 fluorescent dye (Thermo Fisher Scientific). After staining with a mixture of Mowiol and DAPI, samples were analyzed using a Nikon C2 confocal microscope (Nikon, Japan) in 9 planes, after which the stack was projected onto a single plane. DAPI-stained nuclei were used to detect regions of interest (ROI), and number of CBs within each ROI was automatically counted. Counting was performed using ImageJ software; the script is available at: https://github.com/bio-mother/Cajal-bodies-counting-jython-. The staining protocol is detailed in the Supplementary Methods section in the Online Resource 1.

**RT-PCR and qPCR.** For total RNA extraction, HeLa S3 cells were grown to a concentration of 1 million/mL (~40% confluency); cells were collected and resuspended in 300 µL of QIAzol reagent (QIAGEN, Germany) per 1 million cells. RNA samples were extracted according to the manufacturer's instructions.

After removal of genomic DNA using DNase I (Thermo Fisher Scientific), cDNA synthesis was performed using a Maxima First Strand cDNA Synthesis Kit for RT-qPCR (Thermo Fisher Scientific). PCR was performed using a DreamTaq PCR Master Mix (2X) (Thermo Fisher Scientific) according to the recommended protocol; annealing temperature for all primers was 60°C. PCR products were separated on a 1% agarose gel at 200 V. For real-time PCR, a Maxima SYBR Green/ROX qPCR Master Mix (Thermo Fisher Scientific) was used.

**Isolation of a newly synthesized RNA.** Cells were seeded before labeling at a concentration of 1 million/mL. The culture medium was supplemented with 5-ethynyluridine (5-EU) at concentration of 0.5 mM (200 mM 5-EU stock solution in DMSO was stored at −20°C). Cells were incubated with 5-EU for 10 and 20 min. After incubation, cells were collected, separated from the medium, and resuspended in 300 µL of a QIAzol lysis reagent (QIAGEN, Germany) per 1 million cells. RNA samples were extracted according to the manufacturer's instructions. Newly synthesized RNA labeled with 5-EU was purified using a Click-iT™ Nascent RNA Capture Kit (Invitrogen, USA) according to the protocol described previously [30]; a brief description of the protocol is available in the Supplementary Methods section in the Online Resource 1.

**RNA sequencing library preparation.** A NEBNext Ultra II RNA Library Prep Kit for Illumina (NEB, USA) was used for library preparation. Beads were mixed with a first-strand buffer, random primers, and water according to the manufacturer's protocol and incubated at 94°C for 12 min to obtain longer RNA fragments. Subsequent steps were performed according to the manufacturer protocol; the resulting cDNA library was sequenced using an Illumina Hiseq1500 Sequencing System (Illumina, USA).

**High-throughput sequencing data analysis.** Demultiplexed fastq files from Illumina were processed using TrimGalore (version 0.6.6) to remove adapters and low-quality bases from the ends of reads and filter them by a minimum length of 20 nucleotides [31]. After quality control using FastQC (version 0.11.9), human genome GRCh38 indices were generated using STAR (version 2.7.10) -runMode genomeGenerate and gencode annotation (version 42) with parameters twopassMode Basic and others specified in the ENCODE standard long RNA-seq pipeline (see STAR manual) [32, 33]. To identify chimeric reads, default STAR-Fusion parameters were added, including

--chimSegmentMin 12,
--chimJunctionOverhangMin 8,
--chimOutJunctionFormat 1,
--alignSJstitchMismatchNmax 5-1 5 5,
--chimMultimapScoreRange 3,
--chimMultimapNmax 20,
--chimScoreJunctionNonGTAG-4,
--chimNonchimScoreDropMin 10,
--alignInsertionFlush Right.

To estimate the proportion of reads mapping to exons, they were counted on genes using featureCounts from the Rsubread package (v.2.12.0) [34]. Only uniquely aligned reads were retained using samtools (version 1.3.1) -q 255, and those corresponding to small and repetitive RNA genes (including ribosomal, transfer, small nuclear and nucleolar, and microRNAs) were filtered out according to gencode comprehensive (v.42), RNAatlas, UCSC RepeatMasker, sno/miRNA, and tRNA annotations [35-37]. For this, bedtools (version 2.30.0) intersect was used with parameters -split, -v, and -f 0.9 (minimum fraction of the read overlapping with small RNA) [38]. Next, gene and exon coverage were calculated using featureCounts with allowMultiOverlap = T and GTF.featureType = "gene" or GTF.featureType = "exon," respectively, using the same gencode comprehensive annotation as in the alignment step. Finally, genes with a non-zero total read count in each sample and at least 3 cpm (counts per million) in at least one sample were retained.

All plots presented in the article were generated using the R package ggplot2 (version 3.4.0). Principal component analysis was performed using fviz_pca_ind from the R package factoextra (version 1.0.7).

**Splicing rate assessment.** To assess kinetics of splicing at the level of individual donor and acceptor sites, proportion of unspliced reads among all overlapping regions was calculated using the R package FRASER (v.1.10.0) [39]. For this, bam files containing uniquely aligned reads were imported into R using the FraserDataSet function, after which read counting was performed using countRNAData with parameters keepNonStandardChromosomes = FALSE, filter = FALSE, and the genome from the BSgenome. Hsapiens.UCSC.hg38 package (version 1.4.4). Next, for each splicing site, Ψ values were calculated using the calculatePSIValues function by default. These values reflect proportion of unspliced reads overlapping the RNA region of interest among all reads crossing it. Finally, the splicing rate at 10 and 20 min was calculated as 1 − (Ψ_{10 min/20 min} − Ψ_{total RNA}) and adjusted by multiplying by (1 − Ψ_{total RNA}) to account for intron retention events.

**Splicing accuracy assessment.** Splicing accuracy was assessed by calculating the Shannon entropy of Ψ values for 5′ and 3′ splice sites using FRASER (version 1.10.0) [39]; a detailed description of the method is available in the Supplementary Methods section in the Online Resource 1.

**Differential expression analysis.** Differential expression analysis was performed using edgeR (version 3.42.4). Read counts on gene exons were normalized using calcNormFactors, followed by model parameter estimation and testing using estimateDisp, glmQLFit, and glmQLFTest.

Gene set enrichment analysis (GSEA) was performed using the fgsea package (version 1.26.0) for the genes ranked by $\log_2$FC (for differential expression) or negative $\log_{10}$Pv with the sign of deltaPSI (for alternative splicing), using gene sets from MSigDB (2022.1) [40].

We also calculated number of the reads on introns and exons using gencode v.42 annotation with addition of intronic regions, using the featureCounts function with parameters allowMultiOverlap = T and GTF.featureType = “exon” or “intron.” Previously, we filtered out reads mapped to repetitive genes and small RNA genes. Calculation of the number of reads on introns and exons was used to assess changes in the intron and exon expression levels in the Δ*METTL4* cells compared to the wild-type (WT) cells relative to the overall change in gene expression (i.e., to assess changes in intron usage considering differential gene expression). This was done using edgeR (version 3.42.4) in the same way as for differential expression analysis, but using the diffSpliceDGE function.

**Alternative splicing.** Alternative splicing events were identified using rMATS (version 4.1.2) with parameters: -t single, -variable-read-length, -ReadLength 120, and gencode v.42 annotation [41].

Complementarity of the splice sites to snRNA was determined as proposed in Bolikhova et al. [30]; a brief description is available in the Supplementary Methods section in the Online Resource 1.

## RESULTS

**METTL4 methyltransferase is responsible for the formation of $m^6Am30$ in U2 snRNA.** Previous studies have shown that METTL4 methyltransferase in human cells is responsible for formation of $m^6Am$ from Am at position 30 of the spliceosomal U2 snRNA [21, 27]. To confirm this function, we created the HeLa S3 cell line with inactivated *METTL4* gene (HeLa S3 Δ*METTL4*). CRISPR/Cas9 technology and guide RNA targeting exon 4 of the gene were used to create the cell line (the cleavage site was chosen so that a frameshift mutation would eliminate the main structural part of the protein, including the SAM binding site). A monoclonal cell line was selected in which a single nucleotide insertion occurred in both alleles encoding METTL4 (Fig. 1a, “i1”). The high-throughput RNA sequencing data from the HeLa S3 WT and HeLa S3 Δ*METTL4* cells confirmed presence of the insertion in the mRNA encoding METTL4. Western blot analysis confirmed absence of the METTL4 protein in the HeLa S3 Δ*METTL4* cells compared to the wild-type cells (HeLa S3 WT; Fig. 1b). Disappearance of METTL4 did not affect growth rate of the HeLa S3 cells (Fig. S1 in the Online Resource 1). In agreement with the previous studies, inactivation of *METTL4* led to disappearance of one methyl group in the corresponding region of U2 snRNA, as shown by mass spectrometry (Fig. 1c).

**Absence of METTL4 methyltransferase does not affect quantity or localization of the spliceosomal snRNAs.** Modifications could significantly affect processing, localization, and stability of certain RNA groups [42, 43]. Using RT-qPCR, we showed that expression of the U2 snRNA in the HeLa S3 Δ*METTL4* cells does not change compared to the wild type (Fig. 2a). Similarly, expression of other spliceosomal snRNAs does not change with disappearance of METTL4 (Fig. 2a). Localization of various snRNAs also does not depend on the presence of METTL4 in the cell, as shown by RT-qPCR; total RNA for the reaction was isolated separately from the cytoplasm and nuclei of the HeLa S3 WT and HeLa S3 Δ*METTL4* cells (Fig. 2b). Same distribution of the U2 snRNA in both cell lines was additionally confirmed by staining with FISH probes specifically binding to U2 (Fig. 2c).

Part of the U2 snRNA maturation process occurs within Cajal bodies (CBs) – nuclear structures where snRNA modification and final stages of the small nuclear ribonucleoprotein (snRNP) maturation take place [44-46]. It is also known that disruption

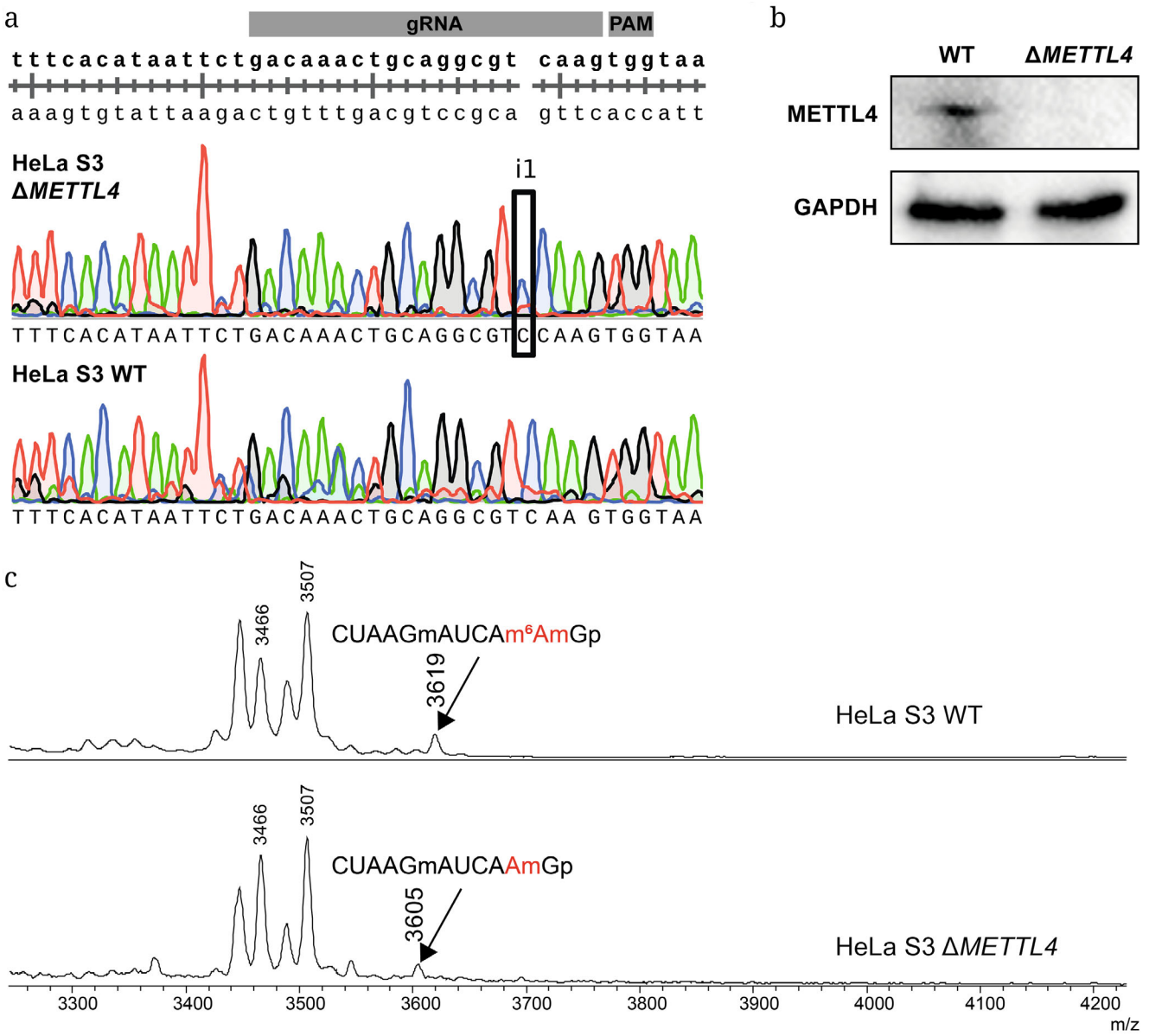


**Fig. 1.** Confirmation of the HeLa S3 Δ*METTL4* phenotype. a) Sanger sequencing of the target region in the *METTL4* gene ("i1" in the cell line with gene inactivation indicates insertion of one nucleotide). gRNA indicates the sequence corresponding to the guide RNA; Protospacer adjacent motif (PAM) is the site recognized by the CRISPR/Cas9 system. b) Amount of METTL4 protein in total lysates of the HeLa S3 WT and HeLa S3 Δ*METTL4* cell lines, shown by Western blotting. GAPDH was used as a loading control. c) Mass spectra of U2 snRNA after RNase T1 treatment. The fragment CUAAGmAUCA $m^6$AmGp (calculated average mass-to-charge ratio (m/z) is 3619) corresponds to the modified form of U2 snRNA; the fragment CUAAGmAUCAAmGp (calculated average m/z is 3619) corresponds to the form without 2′-O-methylation at position 30. Peaks corresponding to these fragments are indicated by arrows on the graph. The spectra reflect disappearance of the modification in the cell line with *METTL4* inactivation.

of snRNP maturation could affect the number of CBs in the cell [47]. The HeLa S3 WT and HeLa S3 Δ*METTL4* cells were stained with antibodies against coilin (a protein that forms the structure of CBs [48]) and DAPI, which stains DNA. By analyzing the number of coilin-positive signals in the 1070 WT and 780 Δ*METTL4* nuclei, we found a significant reduction in the number of such signals in the cells lacking methyltransferase (Fig. 2d and e; images of cells stained for coilin, with nuclei indicated, are available in Fig. S1 in the Online Resource 1).

**Disappearance of METTL4 leads to noticeable changes in gene expression.** Although METTL4 does not directly affect the quantity of snRNAs, changes in the expression levels of various genes are one of the main mechanisms allowing the cell to respond to changing conditions [49]. By performing high-throughput RNA sequencing of the HeLa S3 WT

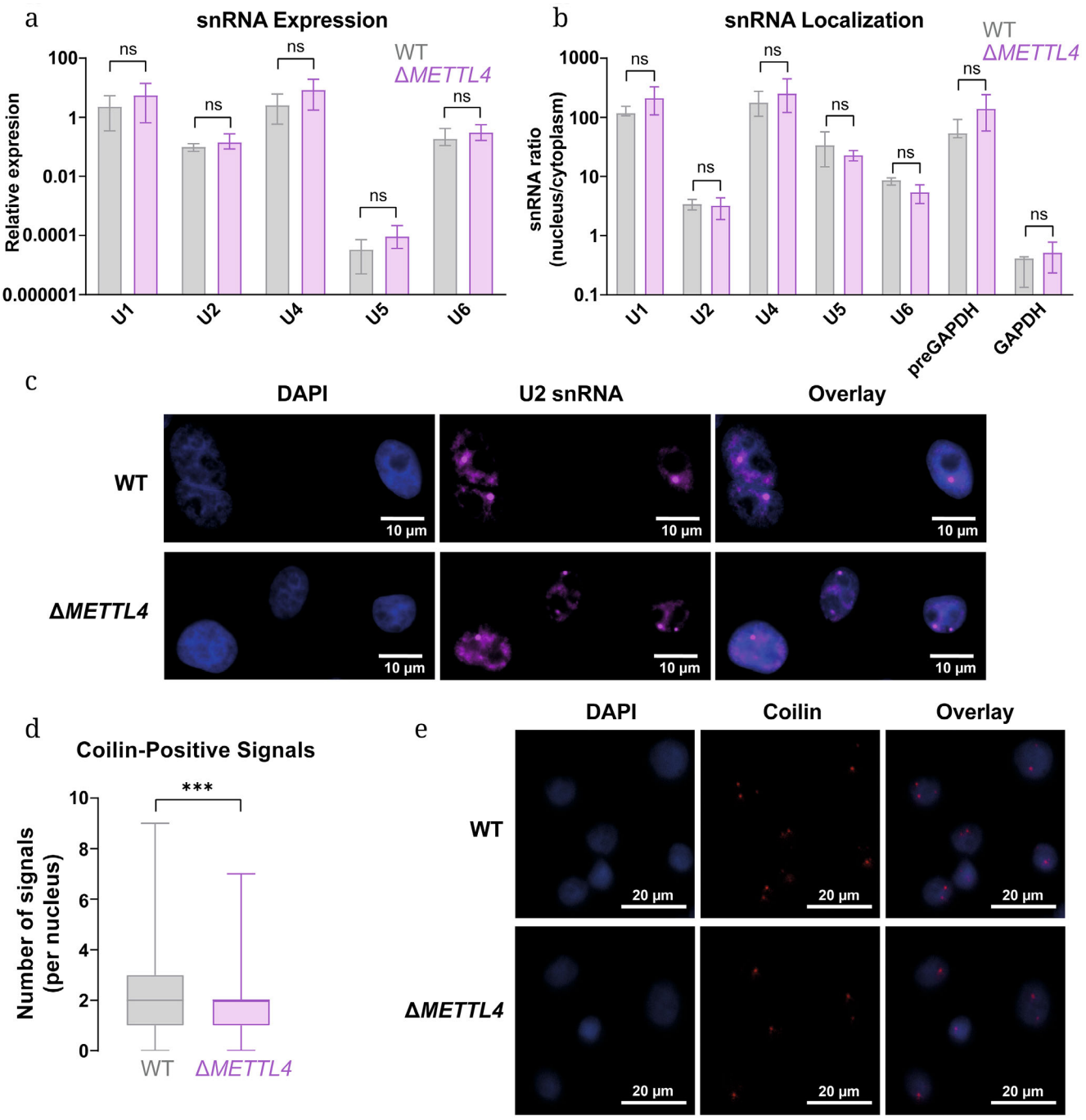


**Fig. 2.** Overall effect of *METTL4* inactivation on quantity and maturation of spliceosomal snRNAs. a) Analysis of snRNA expression in the HeLa S3 WT and HeLa S3 Δ*METTL4* cell lines performed using RT-qPCR. Six biological replicates were used for each cell line. Expression level of the target was normalized to the expression level of the housekeeping gene GAPDH. The graph shows mean expression value and spread of values. Gray bars denote WT, purple bars denote Δ*METTL4*. Statistical significance was determined using the two-sided Mann–Whitney U test; ns, $p > 0.05$. b) Analysis of distribution of spliceosomal snRNAs in the HeLa S3 WT and HeLa S3 Δ*METTL4* cells performed using RT-qPCR. Three biological replicates were used for each cell line. Y-axis shows the ratio of the amount of specific RNA in the nuclear and cytoplasmic fractions. Bars reflect the mean and spread of values. Gray bars denote WT, purple bars denote Δ*METTL4*; ns, $p > 0.05$. c) Micrographs of the HeLa S3 WT and HeLa S3 Δ*METTL4* cells: nuclei stained with DAPI (left panel, blue), U2 snRNA stained with Cy5-labeled FISH probes (middle panel, purple); right panel is a merged image. d) Distribution of the number of coilin-positive signals in the nuclei of the HeLa S3 WT (gray) and HeLa S3 Δ*METTL4* (purple) cells. Sample sizes: 1070 and 780 nuclei for WT and Δ*METTL4*, respectively. Statistical significance was determined using the unpaired Student's *t*-test; *** $p \le 0.001$. e) Micrographs of the HeLa S3 WT and HeLa S3 Δ*METTL4* cells taken in 9 planes and projected onto a single plane: nuclei stained with DAPI (left panel, blue), cells stained with antibodies against coilin (middle panel, purple); the right panel is a merged image.

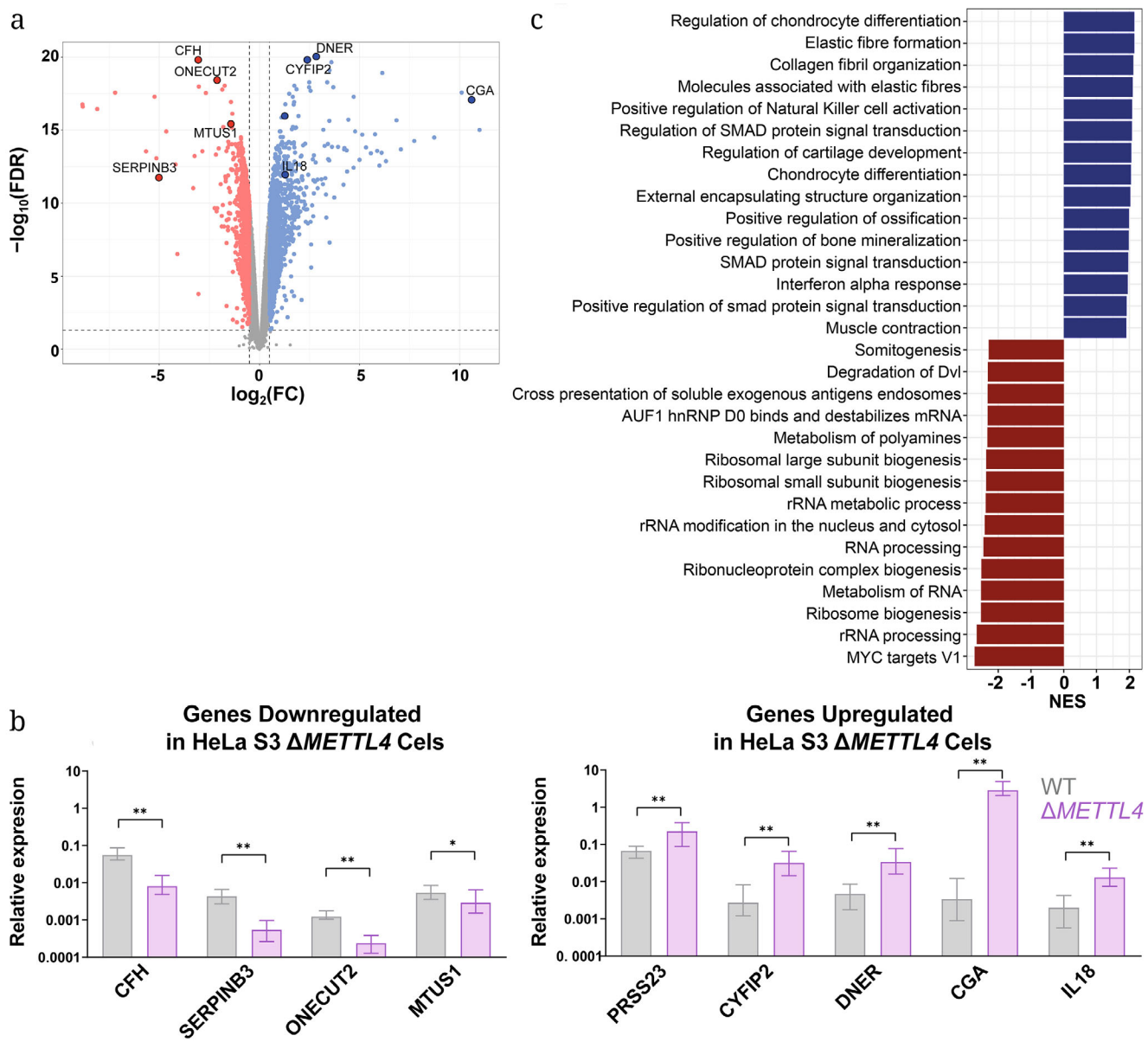


**Fig. 3.** Analysis of expression changes occurring upon *METTL4* inactivation. a) Results of differential expression analysis of 13,813 genes (with cpm ≥ 3 in at least three samples) in the HeLa S3 Δ*METTL4* cells compared to the wild-type cells. Vertical dashed lines correspond to $|\log_2 FC| = 0.5$; horizontal line denotes FDR = 0.05. In total, 1,217 genes are more actively expressed in the Δ*METTL4* cells compared to the wild type (highlighted in blue), and 946 are less actively expressed (highlighted in red). Genes with qPCR-confirmed differential expression are marked with a dark border and additionally labeled. b) Confirmation of high-throughput sequencing results. RT-qPCR was performed in six replicates for each cell line. Expression level of the target gene was normalized to the expression level of the housekeeping gene *GAPDH*. Gray bars denote WT, purple bars denote Δ*METTL4*. Statistical significance was determined using the one-sided Mann-Whitney U test; * $p \le 0.05$, ** $p \le 0.01$. c) Results of gene set enrichment analysis (GSEA) for 15 pathways with increased (blue) and decreased (red) regulation and FDR < 0.05. NES – normalized enrichment score.

and HeLa S3 Δ*METTL4* cells (Fig. S2a, Table S2 in the Online Resource 1) and comparing the obtained transcriptomes, we found a number of genes that are more or less actively expressed in the cells without METTL4 compared to the wild type cells (Fig. 3a); some findings were confirmed using RT-qPCR (Fig. 3b). When conducting gene set enrichment analysis (GSEA) of the differentially expressed genes with gene ontology terms, we found activation of the pathways associated with the development of immune response ("Positive regulation of Natural Killer cell activation" and "Interferon alpha response"; Fig. 3c) in the HeLa S3 Δ*METTL4*. Among the pathways inhibited in the HeLa S3 Δ*METTL4* cells are those associated with RNA processing (e.g., "rRNA metabolic process" and "RNA processing"; Fig. 3c).

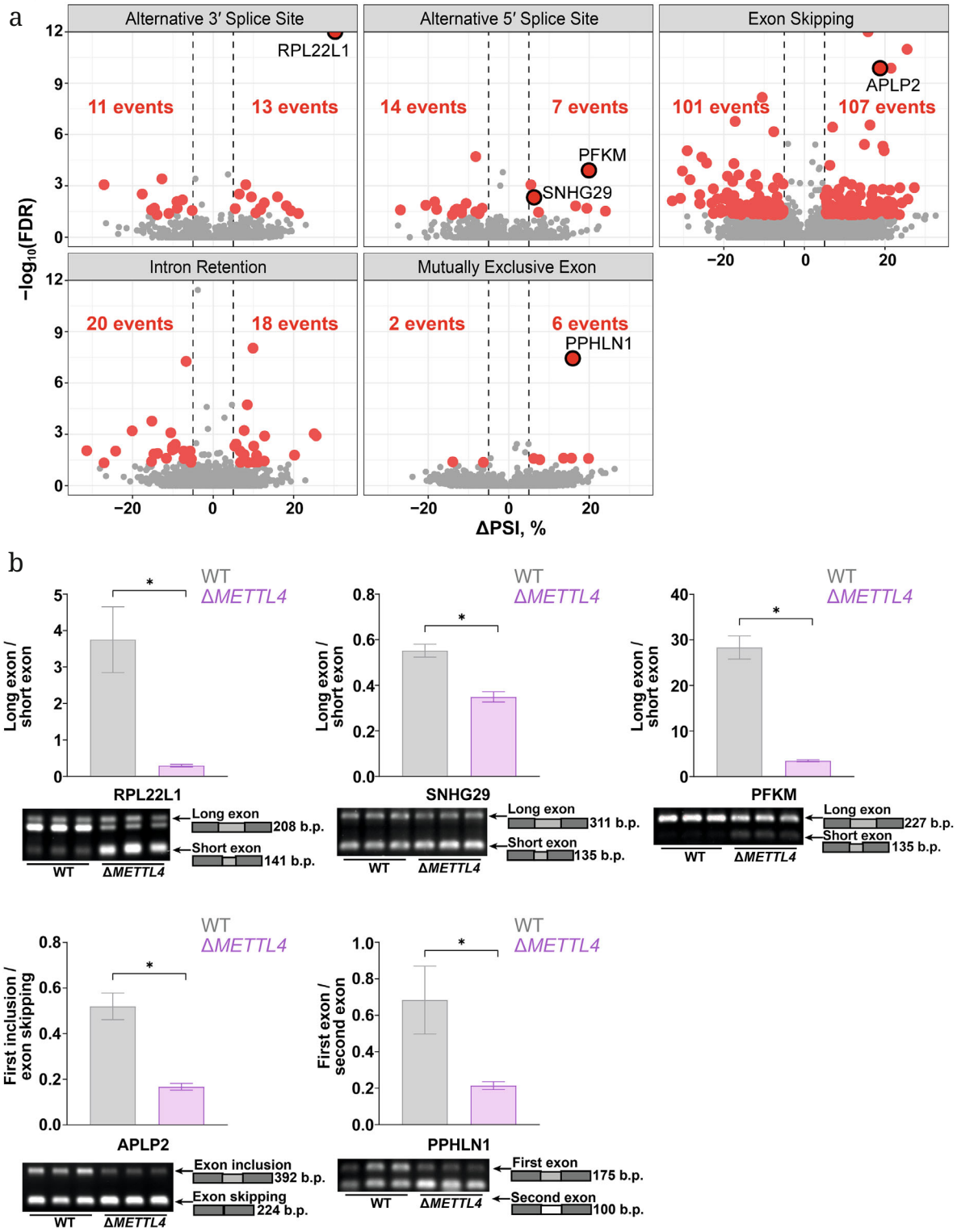


**Fig. 4.** Analysis of alternative splicing in the HeLa S3 Δ*METTL4* cells compared to the wild-type cells. a) Overall changes identified by examining 68,005 alternative splicing events (6,020 alternative 3′ splice sites, 4,046 alternative 5′ splice sites, 45,727 exon skipping events, 4,732 intron retention events, 7,480 mutually exclusive exons), where at least one isoform had coverage of ≥10 reads in all replicates. Red dots indicate events with FDR < 0.05 and |ΔPSI| > 5%. Number of alternative splicing events exceeding the threshold values is indicated in red on the graph. Events successfully confirmed by RT-qPCR are additionally highlighted with a dark border and labeled. b) Confirmation of the high-throughput sequencing results using RT-PCR followed by gel electrophoresis. Each experiment was performed for three biological replicates. For each event, the electrophoresis of RT-PCR products in agarose gel is shown below, and quantitative assessment of the product ratio on the gel is shown above. Gray bars denote WT, purple bars denote Δ*METTL4*. Statistical significance was determined using the one-sided Mann–Whitney U test; * $p \le 0.05$.

**Alternative splicing shifts in the HeLa S3 Δ*METTL4* cells.** Presence of modified bases in spliceosomal snRNAs plays an important role in both regulation of the splice site and branch point recognition, as well as in maintaining interactions that ensure structure of the spliceosome [6]. Earlier studies suggested that modification of A30 in the U2 snRNA specifically affects splicing, as this residue is located immediately before the branch point recognition site [21, 27]. We compared the ratio of alternative splicing products in the HeLa S3 WT and the HeLa S3 Δ*METTL4* cells. The analysis revealed a significant number of differentially spliced genes, some of which were confirmed using RT-PCR (Fig. 4, a and b; Table S3 in the Online Resource 1).

It can be noted that the largest number of events changing upon the *METTL4* inactivation belongs to "Exon Skipping," with both increased inclusion and exclusion of the exon in the HeLa S3 Δ*METTL4* compared to the wild type depending on the specific splicing event.

**Splicing changes in the HeLa S3 Δ*METTL4* cells are general in nature.** Modifications of snRNAs can have both general and specific effects on splicing [6, 13]. We examined which groups of alternative exons are most susceptible to change upon the *METTL4* inactivation. For the alternative exons that are included to a greater, equal, or lesser extent in the HeLa S3 Δ*METTL4* cells in comparison with the wild-type cells, we compared lengths of the exons themselves, as well as of the surrounding introns (Fig. 5a). As a result, it was found that the long alternative exons are on average more represented in the Δ*METTL4* (ΔPSI < −5%), while the short ones are more likely to be excluded in the cells without the methyltransferase (ΔPSI > 5%). At the same time, length of the following intron is slightly greater for the events characterized by exon skipping in the Δ*METTL4*. In the next step, for similar groups of the alternatively spliced exons, we compared complementarity of the 5′ splice site of the upstream and downstream introns to the sequences of U1, U5, and U6 snRNAs, as well as the region including the branch point – U2 snRNA (Fig. S3a and S3b in the Online Resource 1). No significant correlation between complementarity and splicing changes in the Δ*METTL4* was found. A similar analysis was performed for the second most changing group of splicing events – intron retention (Fig. 5b; Fig. S3c in the Online Resource 1). The main and only pattern is that the longer introns are more often retained in the cell line without the METTL4 methyltransferase.

To demonstrate potential functional role of splicing changes, we identified biological processes enriched in the alternatively spliced genes (GSEA); the analysis results are shown in Fig. 5c. As in the case of differential expression, pathways related to RNA maturation and immune response were found. A possible explanation may be that some of the splicing changes are direct consequences of the changes in gene expression upon *METTL4* inactivation, and *vice versa*, that the alternative splicing of certain genes could directly affect expression profile of the cell.

We also determined whether the METTL4 methyltransferase has a general effect on splicing by comparing efficiency and accuracy of splicing of all introns in the cell. As a measure of splicing efficiency, we used the average proportion of exon representation relative to the total gene coverage (Fig. 5d). As a measure of splicing accuracy, the Shannon entropy of Ψ values of 5′ and 3′ splice sites was calculated (see "Materials and Methods" section; Fig. 5e). We showed that the average splicing efficiency decreases upon *METTL4* inactivation (the median proportion of exon reads in total RNA of HeLa S3 WT is 0.9097649, in total RNA of the HeLa S3 Δ*METTL4* it is 0.9001537; $p < 10^{-15}$), but the average splicing accuracy remains unchanged.

**Splicing rate in the HeLa S3 Δ*METTL4* cells is significantly lower than in the wild-type cells.** Splicing is an extremely dynamic process, and changes in it may not be noticeable when considering only total RNA. To determine how METTL4 affects the splicing rate, we used the analysis method described in Bolikhova et al. [30]. Briefly, the newly synthesized RNA after 10 and 20 min of labeling cells with 5-EU was isolated and subjected to high-throughput sequencing (Fig. S2a and S2b in the Online Resource 1). By comparing the degree of splicing of each intron in the newly synthesized RNA separately after 10 and 20 min of labeling and in the poly-A fraction of total RNA (used as an indicator of isoform ratio in mature RNA), we calculated the splicing rate for each donor and acceptor site. The rate values obtained for the RNA after 10 and 20 minutes of labeling were similar (Fig. S2c and S2d in the Online Resource 1), confirming applicability of this method for assessing splicing rate of each site. Analysis of the values for RNA isolated after 10 min of labeling is presented in the main text, and after 20 min in Fig. S4 in the Online Resource 1.

The average splicing rate in the HeLa S3 Δ*METTL4* cell line was lower than in the wild type (Fig. 6a; Fig. S4a in the Online Resource 1). By analogy with the analysis of the total poly-A fraction, we calculated the Shannon entropy of Ψ values of 5′ and 3′ splice sites in the newly synthesized RNA (Fig. 6b; Fig. S4b in the Online Resource 1). As seen in the graphs, in the newly synthesized RNA isolated after 10 min, the splicing accuracy in the Δ*METTL4* is significantly lower than in the wild type (Fig. 6b), but this effect disappears after 20 min of labeling. Thus, only in the "youngest" RNAs the presence of METTL4 does affect splicing accuracy, and this effect is quickly neutralized

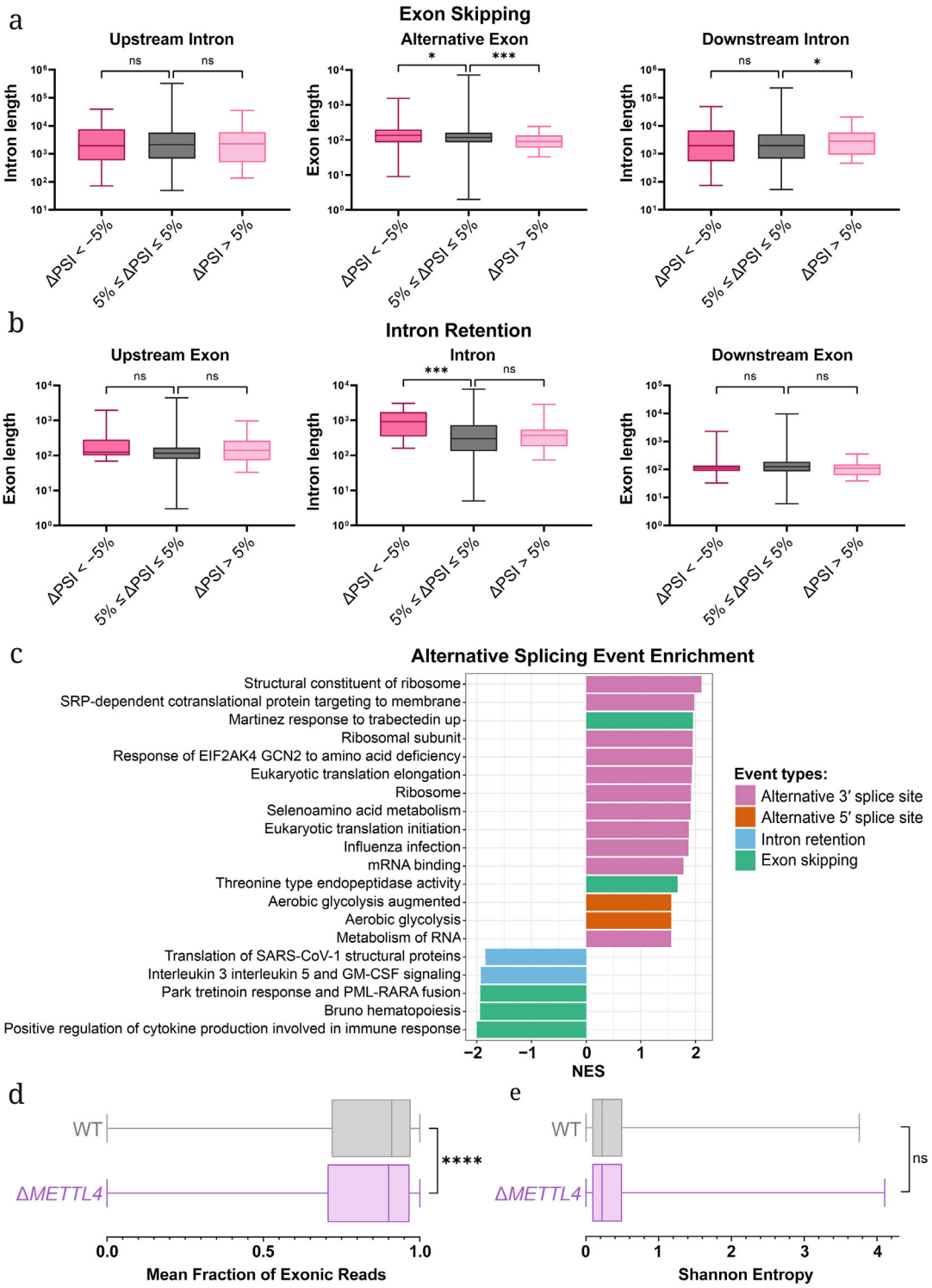


**Fig. 5.** Splicing changes upon *METTL4* inactivation. a) Distribution of lengths of alternatively included exons (central graph), as well as the upstream and downstream introns (left and right graphs, respectively) depending on the degree of inclusion/exclusion of the alternative exon in the HeLa S3 Δ*METTL4* cells compared to the wild type. b) Distribution of lengths of alternative introns (central graph), as well as the upstream and downstream exons (left and right graphs, respectively) depending on the degree of retention of the alternative intron in the HeLa S3 Δ*METTL4* cells compared to the wild type. c) Results of gene set enrichment analysis (GSEA) of alternatively spliced genes with FDR < 0.05. NES, normalized enrichment score. d) Analysis of global splicing efficiency by assessing average proportion of exon representation for 15,035 genes with cpm ≥ 3 in at least three samples. e) Analysis of splicing accuracy through assessment of Shannon entropy of 5′ and 3′ splice site Ψ values. In total, 56,062 splice sites were considered, for each of which the cpm of the splicing product was ≥1 in at least one sample. Statistical significance was determined using the one-sided Wilcoxon rank test; ns, $p > 0.05$; * $p \le 0.05$; *** $p \le 0.001$; **** $p \le 10^{-15}$. Gray color denotes WT, purple denotes Δ*METTL4*.

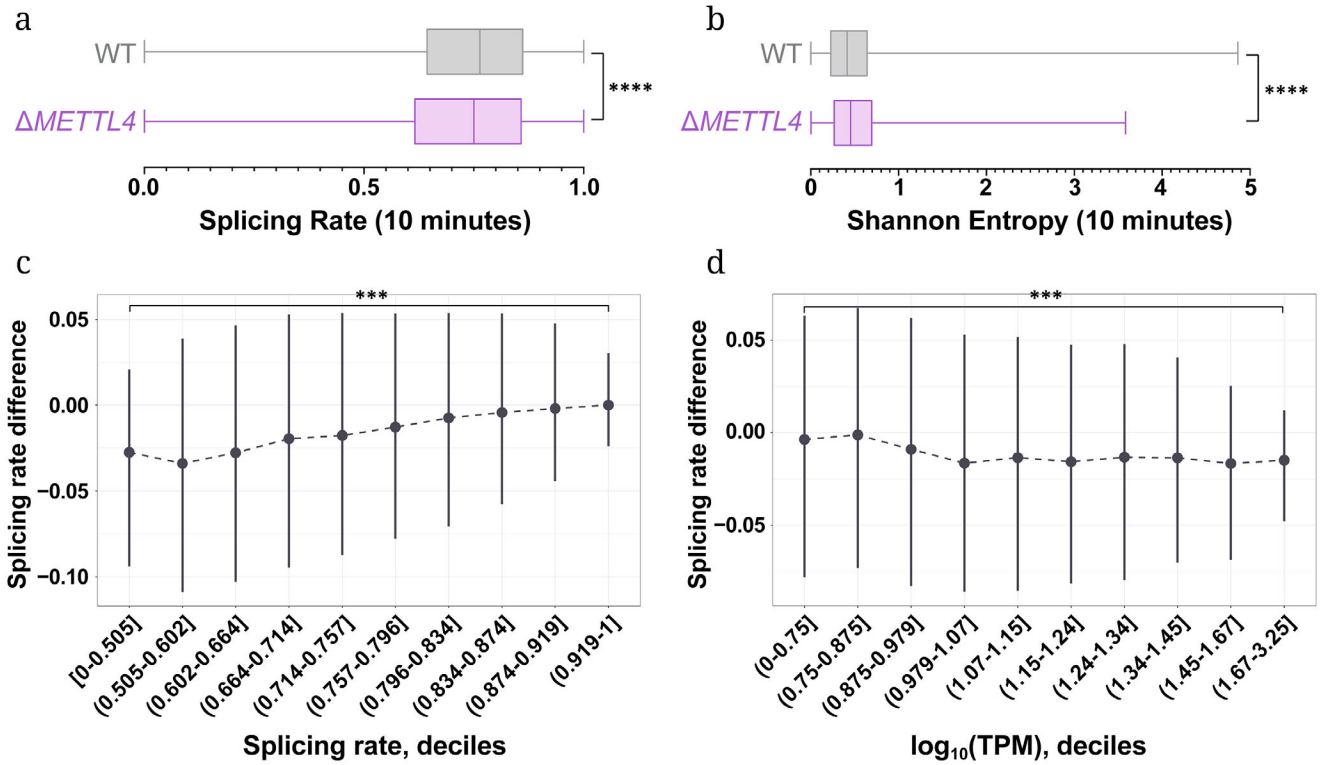


**Fig. 6.** Analysis of splicing rate and accuracy (RNA isolated after 10 min of 5-EU labeling) in the HeLa S3 WT and the HeLa S3 Δ*METTL4* cells. a) Comparison of average splicing rates. Values for 68,288 splice sites are shown, for each of which the cpm of the splicing product is ≥10 in at least three samples. b) Comparison of splicing accuracy through assessment of Shannon entropy of 5′ and 3′ splice sites Ψ values. In total, 10,481 splice sites were considered, for each of which the cpm of the product is ≥1 in at least one sample. Statistical significance was determined using the one-sided Wilcoxon rank test; **** $p \le 10^{-15}$. Gray color denotes WT, purple denotes Δ*METTL4*. c) Relationship between the difference in splicing rates (Δ*METTL4* minus WT) and the average splicing rate (divided into deciles). ART ANOVA $p < 10^{-15}$. d) Relationship between the difference in splicing rates (Δ*METTL4* minus WT) and the expression level of the corresponding genes ($\log_{10}$(TPM), values divided into deciles). ART ANOVA $p < 10^{-15}$. Dots correspond to the median values; the lower and upper error bars show 25% and 75% quantiles, respectively. Dashed line reflects the overall trend of the median. Significances of the Tukey test for the difference between the first and last groups are shown on the graphs (*** $p \le 0.001$).

over time, for example, due to degradation of the incorrectly spliced RNA.

To better understand splicing features in the HeLa S3 Δ*METTL4* line, we performed correlation analysis of the degree of change in the splicing rate with various characteristics of the corresponding introns and exons (only significant results are presented). It was shown that the slow-down of splicing in the absence of METTL4 is more pronounced for the initially “slower” introns (Fig. 6c; Fig. S4c in the Online Resource 1). On the other hand, splicing of the introns that are part of the highly expressed genes, which is initially quite fast [30], slows down slightly more in the absence of METTL4 (Fig. 6d; Fig. S4d in the Online Resource 1).

## DISCUSSION

Modification of snRNAs plays an important role in the regulation of splicing, ensuring correct recognition of introns and maintaining optimal structure of the spliceosome [6, 13, 50]. In this work, we confirmed that the METTL4 methyltransferase catalyzes the N6-methylation of Am at position 30 of the U2 snRNA in human cells [21, 22]. To understand the role of METTL4 methyltransferase in the life of a eukaryotic cell, we analyzed the changes occurring in the HeLa S3 cells after inactivation of the *METTL4* gene. Growth rate of the cells without METTL4 did not differ from growth rate of the wild-type cells, which is consistent with the results previously shown in the HEK293T cell line [27].

Modification of certain RNAs is often a mechanism of post-transcriptional regulation of the expression of the corresponding genes, while changes in the expression level of snRNAs themselves could also be an important factor [51, 52]. We did not find fundamental differences in the expression level of spliceosomal snRNAs between the wild-type cells and the cells without METTL4 (Fig. 2a). Maturation of snRNAs following synthesis is, in turn, a complex,

multi-stage process, part of which occurs in the nucleus and part in the cytoplasm [53-55]. The ratio of the amount of snRNAs in the nucleus and cytoplasm turned out to be independent of METTL4 (Fig. 2, b and c). At the same time, we managed to detect a statistically significant decrease in the number of coilin-positive signals in the HeLa S3 Δ*METTL4* cells compared to the HeLa S3 WT (Fig. 2d). Coilin is a known marker of CBs, but it could also be part of other intranuclear structures – histone locus bodies [56]. Histone locus bodies are non-membrane intranuclear structures that play a role in maturation of the histone mRNAs; CBs are similar structures that play an important role in maturation of the snRNPs [45, 57]. It has been shown that disruption of the final stages of snRNP maturation by reducing the number of proteins involved in this process could lead to the increase in the number of CBs, thereby helping to maintain optimal concentration of the spliceosome components [47]. Decrease in the number of coilin-positive signals hints at the presence of a mechanism by which inactivation of *METTL4* affects maturation of the U2 snRNA, associated with the presence of U2 in CBs. However, one cannot rule out a more complex, possibly not snRNA-mediated, connection between METTL4 and functioning of the histone locus bodies. Thus, this issue requires further study.

The most obvious process that could be affected by snRNA modification is splicing [6]. $m^6Am30$ in the U2 snRNA is located immediately upstream the branch point recognition site [30], while at the later stages of splicing, this residue is located next to the duplex formed by the complementary parts of U2 and U6 [26]. We found that in the cells without METTL4, alternative splicing is significantly altered, with the largest number of events changing upon disappearance of the METTL4 belonging to the exon skipping, and distribution between the more included and excluded exons in the Δ*METTL4* is equally probable (Fig. 4, a and b). It was noted that splicing in the absence of METTL4 proceeds more slowly (Fig. 6a), leading, apparently, to a small but general accumulation of introns for most genes (Fig. 5d). It is important to note the implicit pattern of the splicing slowdown. Initially, the “slower” introns are most susceptible to the disappearance of METTL4 (Fig. 6b; Fig. S3b in the Online Resource 1), which could be explained by less optimized splicing in these regions. However, the RNA molecules of more highly expressed genes, which are normally characterized by increased splicing rates [30], are more susceptible to the slow-down upon *METTL4* inactivation. A possible mechanism partially explaining the observed phenomena may be decrease in the concentration of the mature snRNPs associated with reduction in the number of CBs. Such change in the availability snRNPs would more strongly affect both less efficient splicing sites, which initially attract snRNPs weaker, and the sites of highly represented RNAs, which, due to their greater quantity, require higher concentration of snRNPs to maintain optimal splicing rates.

Modified nucleotides of snRNAs under certain conditions could directly or indirectly regulate transcription [58, 59]. In the HeLa S3 Δ*METTL4* cells, we observe a decrease in the expression of a number of genes associated with rRNA maturation compared to the wild type. It should be noted that small nucleolar RNAs (snoRNAs), such as U3, also pass through CBs during their maturation [48, 60]. At the same time, snoRNAs play an important role in the maturation of ribosome subunits [61-63], which could explain connection between the disruption of snRNA maturation and inhibition of the expression of genes associated with rRNA maturation. At the same time, in the cells with *METTL4* inactivation, more active expression of a group of genes involved in the development of inflammatory response is observed. A similar effect in response to the inhibition of splicing, leading to increase in the amount of intracellular double-stranded RNA due to hybridization of the repetitive elements within introns, has been described in the literature before [64].

In summary, inactivation of the *METTL4* gene in the HeLa S3 cells leads to disruption of the U2 snRNA maturation and, through a previously unstudied mechanism, causes decrease in the number of coilin-positive signals in the cells, which may affect expression of the genes associated with rRNA maturation. At the same time, the Δ*METTL4* cells exhibit decrease in the splicing rate, theoretically explained both by the decrease in concentration of the mature snRNPs, including due to the reduction in the CB number, and by the “imbalance” of the spliceosome due to the disappearance of the N6-methyl group of Am at position 30 of the U2 snRNA.

## CONCLUSION

N6-methylation of adenosine, leading to formation of $m^6A$, is an extremely common modification found in various types of eukaryotic RNA. $m^6A$ can both perform a regulatory function, affecting stability and transport of mRNA, and play a structural role, for example, for nucleotides that are part of ribosomes. In this work, we studied the role of the METTL4 methyltransferase, one of whose most conserved functions is N6-methylation of Am at position 30 of the U2 snRNA.

We showed that disappearance of METTL4 in the HeLa S3 cells leads to a slow-down in splicing, thereby causing intron accumulation. A possible reason for the slow-down in splicing is disruption

of snRNP maturation associated with the decrease in the number of CBs. Another possible consequence of the decrease in the number of CBs is reduction in concentration of the RNA genes associated with rRNA maturation, also observed in the cells without METTL4.

Although importance of METTL4 for splicing efficiency in the HeLa S3 cells is clear, the exact mechanism linking methylation, splicing, and maturation of various RNAs remains to be investigated.

**Abbreviations**

| | |
|---|---|
| 5-EU | 5-ethynyluridine |
| Am | 2′-O-methyladenosine |
| CBs | Cajal bodies |
| gRNA | Guide RNA |
| $m^6A$ | N6-methyladenosine |
| $m^6Am$ | N6,2′-O-dimethyladenosine |
| qPCR | quantitative polymerase chain reaction |
| RT-qPCR | reverse transcription quantitative PCR |
| snRNA | small nuclear RNA |
| snRNP | small nuclear ribonucleoprotein |

**Supplementary information**

The online version contains supplementary material available at https://doi.org/10.1134/S0006297925602382.

**Acknowledgments**

We are grateful to the Lomonosov Moscow State University Development Program for providing access to the Celena X multiparametric cell analysis system.

**Contributions**

A. K. Bolikhova and A. I. Buyan designed and conducted experiments, analyzed data, and wrote the manuscript. M. A. Khokhlova conducted experiments and analyzed data. S. S. Mariasina designed and conducted experiments, analyzed data, and wrote the manuscript. A. R. Izzi, A. Y. Rudenko, M. V. Serebryakova, and A. M. Mazur conducted experiments. O. A. Dontsova supervised the work. P. V. Sergiev supervised the work, conceptualized the study, and wrote the manuscript.

**Funding**

This research was financially supported by the state assignment of Lomonosov Moscow State University. The experimental work was supported by the Russian Science Foundation (grant no. 21-64-00006-P).

**Ethics approval and consent to participate**

This work does not contain any studies involving human and animal subjects.

**Conflict of interest**

The authors of this work declare that they have no conflicts of interest.

## REFERENCES

1. Jiang, X., Liu, B., Nie, Z., Duan, L., Xiong, Q., Jin, Z., Yang, C., and Chen, Y. (2021) The role of m6A modification in the biological functions and diseases, *Signal Transduct. Target. Ther.*, **6**, 74, https://doi.org/10.1038/s41392-020-00450-x.
2. Boo, S. H., and Kim, Y. K. (2020) The emerging role of RNA modifications in the regulation of mRNA stability, *Exp. Mol. Med.*, **52**, 400-408, https://doi.org/10.1038/s12276-020-0407-z.
3. Suzuki, T. (2021) The expanding world of tRNA modifications and their disease relevance, *Nat. Rev. Mol. Cell Biol.*, **22**, 375-392, https://doi.org/10.1038/s41580-021-00342-0.
4. Sergiev, P. V., Aleksashin, N. A., Chugunova, A. A., Polikanov, Y. S., and Dontsova, O. A. (2018) Structural and evolutionary insights into ribosomal RNA methylation, *Nat. Chem. Biol.*, **14**, 226-235, https://doi.org/10.1038/nchembio.2569.
5. Kazimierczyk, M., and Wrzesinski, J. (2021) Long non-coding RNA epigenetics, *Int. J. Mol. Sci.*, **22**, 6166, https://doi.org/10.3390/IJMS22116166.
6. Morais, P., Adachi, H., and Yu, Y. T. (2021) Spliceosomal snRNA epitranscriptomics, *Front. Genet.*, **12**, 652129, https://doi.org/10.3389/FGENE.2021.652129/XML.
7. Louloupi, A., Ntini, E., Conrad, T., and Ørom, U. A. V. (2018) Transient N-6-methyladenosine transcriptome sequencing reveals a regulatory role of m6A in splicing efficiency, *Cell. Rep.*, **23**, 3429-3437, https://doi.org/10.1016/j.celrep.2018.05.077.
8. Wang, X., Zhao, B. S., Roundtree, I. A., Lu, Z., Han, D., Ma, H., Weng, X., Chen, K., Shi, H., and He, C. (2015) N6-methyladenosine modulates messenger RNA translation efficiency, *Cell*, **161**, 1388-1399, https://doi.org/10.1016/j.cell.2015.05.014.
9. Wang, X., Lu, Z., Gomez, A., Hon, G. C., Yue, Y., Han, D., Fu, Y., Parisien, M., Dai, Q., Jia, G., Ren, B., Pan, T., and He, C. (2013) N6-methyladenosine-dependent regulation of messenger RNA stability, *Nature*, **505**, 117-120, https://doi.org/10.1038/nature12730.
10. Peng, H., Chen, B., Wei, W., Guo, S., Han, H., Yang, C., Ma, J., Wang, L., Peng, S., Kuang, M., and Lin, S. (2022) N6-methyladenosine (m6A) in 18S rRNA promotes fatty acid metabolism and oncogenic transformation, *Nat. Metab.*, **4**, 1041-1054, https://doi.org/10.1038/s42255-022-00622-9.
11. Ma, H., Wang, X., Cai, J., Dai, Q., Natchiar, S. K., Lv, R., Chen, K., Lu, Z., Chen, H., Shi, Y. G., Lan, F., Fan, J., Klaholz, B. P., Pan, T., Shi, Y., and He, C. (2019) N 6-Methyladenosine methyltransferase ZCCHC4 mediates ribosomal RNA methylation, *Nat. Chem. Biol.*, **15**, 88-94, https://doi.org/10.1038/S41589-018-0184-3.
12. Warda, A. S., Kretschmer, J., Hackert, P., Lenz, C., Urlaub, H., Höbartner, C., Sloan, K. E., and Bohnsack, M. T. (2017) Human METTL16 is a N6-methyladenos-

ine (m6A) methyltransferase that targets pre-mRNAs and various non-coding RNAs, *EMBO Rep.*, **18**, 2004-2014, https://doi.org/10.15252/EMBR.201744940.
13. Ishigami, Y., Ohira, T., Isokawa, Y., Suzuki, Y., and Suzuki, T. (2021) A single m6A modification in U6 snRNA diversifies exon sequence at the 5′ splice site, *Nat. Commun.*, **12**, 3244, https://doi.org/10.1038/s41467-021-23457-6.
14. Yang, Y., Hsu, P. J., Chen, Y. S., and Yang, Y. G. (2018) Dynamic transcriptomic m6A decoration: Writers, erasers, readers and functions in RNA metabolism, *Cell. Res.*, **28**, 616-624, https://doi.org/10.1038/S41422-018-0040-8,.
15. Liu, J., Yue, Y., Han, D., Wang, X., Fu, Y., Zhang, L., Jia, G., Yu, M., Lu, Z., Deng, X., Dai, Q., Chen, W., and He, C. (2014) A METTL3-METTL14 complex mediates mammalian nuclear RNA N6-adenosine methylation, *Nat. Chem. Biol.*, **10**, 93-95, https://doi.org/10.1038/nchembio.1432.
16. Lai, J. C. Y., Hsu, K. W., and Wu, K. J. (2024) Interrogation of the interplay between DNA N6-methyladenosine (6mA) and hypoxia-induced chromatin accessibility by a randomized empirical model (EnrichShuf), *Nucleic Acids Res.*, **52**, 13605-13624, https://doi.org/10.1093/NAR/GKAE1152.
17. Hsu, K. W., Lai, J. C., Chang, J. S., Peng, P. H., Huang, C. H., Lee, D. Y., Tsai, Y. C., Chung, C. J., Chang, H., Chang, C. H., Chen, J. L., Pang, S. T., Hao, Z., Cui, X. L., He, C., and Wu, K. J. (2022) METTL4-mediated nuclear N6-deoxyadenosine methylation promotes metastasis through activating multiple metastasis-inducing targets, *Genome. Biol.*, **23**, 249, https://doi.org/10.1186/s13059-022-02819-3.
18. Zheng, L., Chen, X., He, X., Wei, H., Li, X., Tan, Y., Min, J., Chen, M., Zhang, Y., Dong, M., Yin, Q., Xue, M., Zhang, L., Huo, D., Jiang, H., Li, T., Li, F., Wang, X., Li, X., and Chen, H. (2025) METTL4-Mediated mitochondrial DNA N6-methyldeoxyadenosine promoting macrophage inflammation and atherosclerosis, *Circulation*, **151**, 946-965, https://doi.org/10.1161/CIRCULATIONAHA.124.069574.
19. Sang, A., Zhang, J., Zhang, M., Xu, D., Xuan, R., Wang, S., Song, X., and Li, X. (2024) METTL4 mediated-N6-methyladenosine promotes acute lung injury by activating ferroptosis in alveolar epithelial cells, *Free Radic. Biol. Med.*, **213**, 90-101, https://doi.org/10.1016/j.freeradbiomed.2024.01.013.
20. Van den Homberg, D. A. L., van der Kwast, R. V. C. T., Quax, P. H. A., and Nossent, A. Y. (2022) N-6-methyladenosine in vasoactive microRNAs during hypoxia; a novel role for METTL4, *Int. J. Mol. Sci.*, **23**, 1057, https://doi.org/10.3390/IJMS23031057.
21. Chen, H., Gu, L., Orellana, E. A., Wang, Y., Guo, J., Liu, Q., Wang, L., Shen, Z., Wu, H., Gregory, R. I., Xing, Y., and Shi, Y. (2020) METTL4 is an snRNA m6Am methyltransferase that regulates RNA splicing, *Cell. Res.*, **30**, 544-547, https://doi.org/10.1038/S41422-019-0270-4,.
22. Luo, Q., Mo, J., Chen, H., Hu, Z., Wang, B., Wu, J., Liang, Z., Xie, W., Du, K., Peng, M., Li, Y., Li, T., Zhang, Y., Shi, X., Shen, W. H., Shi, Y., Dong, A., Wang, H., and Ma, J. (2022) Structural insights into molecular mechanism for N6-adenosine methylation by MT-A70 family methyltransferase METTL4, *Nat. Commun.*, **13**, 5636, https://doi.org/10.1038/s41467-022-33277-x.
23. Gu, L., Wang, L., Chen, H., Hong, J., Shen, Z., Dhall, A., Lao, T., Liu, C., Wang, Z., Xu, Y., Tang, H. W., Chakraborty, D., Chen, J., Liu, Z., Rogulja, D., Perrimon, N., Wu, H., and Shi, Y. (2020) CG14906 (mettl4) mediates m6A methylation of U2 snRNA in *Drosophila*, *Cell Discov.*, **6**, 44, https://doi.org/10.1038/s41421-020-0178-7.
24. Sendinc, E., and Shi, Y. (2023) RNA m6A methylation across the transcriptome, *Mol. Cell.*, **83**, 428-441, https://doi.org/10.1016/j.molcel.2023.01.006.
25. Van der Feltz, C., and Hoskins, A. A. (2019) Structural and functional modularity of the U2 snRNP in pre-mRNA splicing, *Crit. Rev. Biochem. Mol. Biol.*, **54**, 443-465, https://doi.org/10.1080/10409238.2019.1691497.
26. Karunatilaka, K. S., and Rueda, D. (2014) Post-transcriptional modifications modulate conformational dynamics in human U2-U6 snRNA complex, *RNA*, **20**, 16-23, https://doi.org/10.1261/RNA.041806.113.
27. Goh, Y. T., Koh, C. W. Q., Sim, D. Y., Roca, X., and Goh, W. S. S. (2020) METTL4 catalyzes m6Am methylation in U2 snRNA to regulate pre-mRNA splicing, *Nucleic Acids Res.*, **48**, 9250-9261, https://doi.org/10.1093/NAR/GKAA684.
28. Ran, F. A., Hsu, P. D., Wright, J., Agarwala, V., Scott, D. A., and Zhang, F. (2013) Genome engineering using the CRISPR-Cas9 system, *Nat. Protoc.*, **8**, 2281-2308, https://doi.org/10.1038/nprot.2013.143.
29. Laptev, I., Shvetsova, E., Levitskii, S., Serebryakova, M., Rubtsova, M., Zgoda, V., Bogdanov, A., Kamenski, P., Sergiev, P., and Dontsova, O. (2020) METTL15 interacts with the assembly intermediate of murine mitochondrial small ribosomal subunit to form m4C840 12S rRNA residue, *Nucleic Acids Res.*, **48**, 8022-8034, https://doi.org/10.1093/NAR/GKAA522.
30. Bolikhova, A. K., Buyan, A. I., Mariasina, S. S., Rudenko, A. Y., Chekh, D. S., Mazur, A. M., Prokhortchouk, E. B., Dontsova, O. A., and Sergiev, P. V. (2024) Study of the RNA splicing kinetics via *in vivo* 5-EU labeling, *RNA*, **30**, 1356-1373, https://doi.org/10.1261/rna.079937.123.
31. Krueger, F., James, F., Ewels, P., Afyounian, E., Weinstein, M., Schuster-Boeckler, B., Hulselmans, G., sclamons (2023) FelixKrueger/TrimGalore: version 0.6.8, https://doi.org/10.5281/ZENODO.7579519.
32. Dobin, A., Davis, C. A., Schlesinger, F., Drenkow, J., Zaleski, C., Jha, S., Batut, P., Chaisson, M., and Gingeras, T. R. (2013) STAR: Ultrafast universal RNA-seq aligner,

*Bioinformatics*, **29**, 15-21, https://doi.org/10.1093/BIOINFORMATICS/BTS635.

33. Loveland, J. E., Mudge, J. M., Sisu, C., Wright, J. C., Armstrong, J., Barnes, I., Berry, A., Bignell, A., Boix, C., Carbonell Sala, S., Cunningham, F., Di Domenico, T., Donaldson, S., Fiddes, I. T., García Girón, C., Gonzalez, J. M., Grego, T., Hardy, M., Hourlier, T., Howe, K., Hunt, T., et al. (2021) GENCODE, *Nucleic Acids Res.*, **49**, D916-D923, https://doi.org/10.1093/NAR/GKAA1087.
34. Liao, Y., Smyth, G. K., and Shi, W. (2019) The R package Rsubread is easier, faster, cheaper and better for alignment and quantification of RNA sequencing reads, *Nucleic Acids Res.*, **47**, e47, https://doi.org/10.1093/NAR/GKZ114.
35. Danecek, P., Bonfield, J. K., Liddle, J., Marshall, J., Ohan, V., Pollard, M. O., Whitwham, A., Keane, T., McCarthy, S. A., Davies, R. M., and Li, H. (2021) Twelve years of SAMtools and BCFtools, *Gigascience*, **10**, giab008, https://doi.org/10.1093/GIGASCIENCE/GIAB008.
36. Lorenzi, L., Chiu, H. S., Avila Cobos, F., Gross, S., Volders, P. J., Cannoodt, R., Nuytens, J., Vanderheyden, K., Anckaert, J., Lefever, S., Tay, A. P., de Bony, E. J., Trypsteen, W., Gysens, F., Vromman, M., Goovaerts, T., Hansen, T. B., Kuersten, S., Nijs, N., Taghon, T., Vermaelen, K., Bracke, K., Saeys, Y., Meyer, T., Deshpandeet, N., et al. (2021) The RNA Atlas expands the catalog of human non-coding RNAs, *Nat. Biotechnol.*, **39**, 1453-1465, https://doi.org/10.1038/S41587-021-00936-1.
37. Karolchik, D., Hinrichs, A. S., Furey, T. S., Roskin, K. M., Sugnet, C. W., Haussler, D., and Kent, W. J. (2004) The UCSC table browser data retrieval tool, *Nucleic Acids Res.*, **32**, D493-D496, https://doi.org/10.1093/NAR/GKH103.
38. Quinlan, A. R., and Hall, I. M. (2010) BEDTools: A flexible suite of utilities for comparing genomic features, *Bioinformatics*, **26**, 841-842, https://doi.org/10.1093/BIOINFORMATICS/BTQ033.
39. Mertes, C., Scheller, I. F., Yépez, V. A., Çelik, M. H., Liang, Y., Kremer, L. S., Gusic, M., Prokisch, H., and Gagneur, J. (2022) Author Correction: Detection of aberrant splicing events in RNA-seq data using FRASER, *Nat. Commun.*, **13**, 3474, https://doi.org/10.1038/S41467-022-31242-2.
40. Subramanian, A., Kuehn, H., Gould, J., Tamayo, P., and Mesirov, J. P. (2007) GSEA-P: A desktop application for gene set enrichment analysis, *Bioinformatics*, **23**, 3251-3253, https://doi.org/10.1093/bioinformatics/btm369.
41. Wang, Y., Xie, Z., Kutschera, E., Adams, J. I., Kadash-Edmondson, K. E., and Xing, Y. (2024) rMATS-turbo: an efficient and flexible computational tool for alternative splicing analysis of large-scale RNA-seq data, *Nat. Protoc.*, **19**, 1083-1104, https://doi.org/10.1038/S41596-023-00944-2.
42. Lirussi, L., Demir, Ö., You, P., Sarno, A., Amaro, R. E., and Nilsen, H. (2021) RNA metabolism guided by RNA modifications: the role of SMUG1 in rRNA quality control, *Biomolecules*, **11**, 76, https://doi.org/10.3390/BIOM11010076.
43. Qiu, L., Jing, Q., Li, Y., and Han, J. (2023) RNA modification: mechanisms and therapeutic targets, *Mol. Biomed.*, **4**, 25, https://doi.org/10.1186/S43556-023-00139-X.
44. Darzacq, X., Jády, B. E., Verheggen, C., Kiss, A. M., Bertrand, E., and Kiss, T. (2002) Cajal body-specific small nuclear RNAs: a novel class of 2′-O-methylation and pseudouridylation guide RNAs, *EMBO J.*, **21**, 2746-2756, https://doi.org/10.1093/EMBOJ/21.11.2746.
45. Nesic, D., Tanackovic, G., and Krämer, A. (2004) A role for Cajal bodies in the final steps of U2 snRNP biogenesis, *J. Cell Sci.*, **117**, 4423-4433, https://doi.org/10.1242/JCS.01308.
46. Staněk, D. (2017) Cajal bodies and snRNPs – friends with benefits, *RNA Biol.*, **14**, 671-679, https://doi.org/10.1080/15476286.2016.1231359.
47. Novotný, I., Malinová, A., Stejskalová, E., Matějů, D., Klimešová, K., Roithová, A., Švéda, M., Knejzlík, Z., and Staněk, D. (2014) SART3-dependent accumulation of incomplete spliceosomal snRNPs in Cajal bodies, *Cell Rep.*, **10**, 429-440, https://doi.org/10.1016/j.celrep.2014.12.030.
48. Staněk, D. (2023) Coilin and Cajal bodies, *Nucleus*, **14**, 2256036, https://doi.org/10.1080/19491034.2023.2256036.
49. Casamassimi, A., and Ciccodicola, A. (2019) Transcriptional regulation: molecules, involved mechanisms, and misregulation, *Int. J. Mol. Sci.*, **20**, 1281, https://doi.org/10.3390/IJMS20061281.
50. Duchemin, A., O'Grady, T., Hanache, S., Mereau, A., Thiry, M., Wacheul, L., Michaux, C., Perpète, E., Hervouet, E., Peixoto, P., Ernst, F. G. M., Audic, Y., Dequiedt, F., Lafontaine, D. L. J., and Mottet, D. (2021) DHX15-independent roles for TFIP11 in U6 snRNA modification, U4/U6.U5 tri-snRNP assembly and pre-mRNA splicing fidelity, *Nat. Commun.*, **12**, 6648, https://doi.org/10.1038/s41467-021-26932-2.
51. Vazquez-Arango, P., and O'Reilly, D. (2018) Variant snRNPs: new players within the spliceosome system, *RNA Biol.*, **15**, 17-25, https://doi.org/10.1080/15476286.2017.1373238.
52. Devany, E., Park, J. Y., Murphy, M. R., Zakusilo, G., Baquero, J., Zhang, X., Hoque, M., Tian, B., and Kleiman, F. E. (2016) Intronic cleavage and polyadenylation regulates gene expression during DNA damage response through U1 snRNA, *Cell Discov.*, **2**, 16013, https://doi.org/10.1038/celldisc.2016.13.
53. Köhler, A., and Hurt, E. (2007) Exporting RNA from the nucleus to the cytoplasm, *Nat. Rev. Mol. Cell Biol.*, **8**, 761-773, https://doi.org/10.1038/nrm2255.

54. Pánek, J., Roithová, A., Radivojević, N., Sýkora, M., Prusty, A. B., Huston, N., Wan, H., Pyle, A. M., Fischer, U., and Staněk, D. (2023) The SMN complex drives structural changes in human snRNAs to enable snRNP assembly, *Nat. Commun.*, **14**, 6580, https://doi.org/10.1038/s41467-023-42324-0.
55. Zieve, G. W. (1987) Cytoplasmic maturation of the snRNAs, *J. Cell Physiol.*, **131**, 247-254, https://doi.org/10.1002/JCP.1041310215.
56. Nizami, Z., Deryusheva, S., and Gall, J. G. (2010) The Cajal body and histone locus body, *Cold Spring Harb. Perspect. Biol.*, **2**, a000653, https://doi.org/10.1101/CSHPERSPECT.A000653.
57. Geisler, M. S., Kemp, J. P., and Duronio, R. J. (2023) Histone locus bodies: a paradigm for how nuclear biomolecular condensates control cell cycle regulated gene expression, *Nucleus*, **14**, 2293604, https://doi.org/10.1080/19491034.2023.2293604.
58. Mauer, J., Sindelar, M., Despic, V., Guez, T., Hawley, B. R., Vasseur, J. J., Rentmeister, A., Gross, S. S., Pellizzoni, L., Debart, F., Goodarzi, H., and Jaffrey, S. R. (2019) FTO controls reversible m6Am RNA methylation during snRNA biogenesis, *Nat. Chem. Biol.*, **15**, 340-347, https://doi.org/10.1038/S41589-019-0231-8.
59. Karijolich, J., Kantartzis, A., and Yu, Y. T. (2010) RNA modifications: a mechanism that modulates gene expression, *Methods Mol. Biol.*, **629**, 1-19, https://doi.org/10.1007/978-1-60761-657-3_1.
60. Verheggen, C., Lafontaine, D. L., Samarsky, D., Mouaikel, J., Blanchard, J. M., Bordonné, R., and Bertrand, E. (2002) Mammalian and yeast U3 snoRNPs are matured in specific and related nuclear compartments, *EMBO J.*, **21**, 2736-2745, https://doi.org/10.1093/EMBOJ/21.11.2736.
61. Dragon, F., Gallagher, J. E., Compagnone-Post, P. A., Mitchell, B. M., Porwancher, K. A., Wehner, K. A., Wormsley, S., Settlage, R. E., Shabanowitz, J., Osheim, Y., Beyer, A. L., Hunt, D. F., and Baserga, S. J. (2002) A large nucleolar U3 ribonucleoprotein required for 18S ribosomal RNA biogenesis, *Nature*, **417**, 967-970, https://doi.org/10.1038/nature00769.
62. Kass, S., Tyc, K., Steitz, J. A., and Sollner-Webb, B. (1990) The U3 small nucleolar ribonucleoprotein functions in the first step of preribosomal RNA processing, *Cell*, **60**, 897-908, https://doi.org/10.1016/0092-8674(90)90338-F.
63. Lackmann, F., Belikov, S., Burlacu, E., Granneman, S., and Wieslander, L. (2018) Maturation of the 90S pre-ribosome requires Mrd1 dependent U3 snoRNA and 35S pre-rRNA structural rearrangements, *Nucleic Acids Res.*, **46**, 3692-3706, https://doi.org/10.1093/nar/GKY036.
64. Bowling, E. A., Wang, J. H., Gong, F., Wu, W., Neill, N. J., Kim, I. S., Tyagi, S., Orellana, M., Kurley, S. J., Dominguez-Vidaña, R., Chung, H. C., Hsu, T. Y., Dubrulle, J., Saltzman, A. B., Li, H., Meena, J. K., Canlas, G. M., Chamakuri, S., Singh, S., Simon, L. M., Olson, C., Dobrolecki, L., Lewis, M., Zhang, B., Golding, I., Rosen, J. M., Young, D. W., Malovannaya, A., Stossi, F. Miles, G. et al. (2021) Spliceosome-targeted therapies trigger an antiviral immune response in triple-negative breast cancer, *Cell*, **184**, 384-403, https://doi.org/10.1016/j.cell.2020.12.031.